



**HAL**  
open science

## Retrieval of average CO<sub>2</sub> fluxes by combining in situ CO<sub>2</sub> measurements and backscatter lidar information

Fabien Gibert, Martina Schmidt, Juan Cuesta, Philippe Ciais, Michel Ramonet, Irène Xueref, Eric Larmanou, Pierre Henri Flamant

► **To cite this version:**

Fabien Gibert, Martina Schmidt, Juan Cuesta, Philippe Ciais, Michel Ramonet, et al.. Retrieval of average CO<sub>2</sub> fluxes by combining in situ CO<sub>2</sub> measurements and backscatter lidar information. *Journal of Geophysical Research*, 2007, 112 (D10301), pp.1-16. 10.1029/2006JD008190 . hal-01191971

**HAL Id: hal-01191971**

**<https://hal.science/hal-01191971>**

Submitted on 6 May 2021

**HAL** is a multi-disciplinary open access archive for the deposit and dissemination of scientific research documents, whether they are published or not. The documents may come from teaching and research institutions in France or abroad, or from public or private research centers.

L'archive ouverte pluridisciplinaire **HAL**, est destinée au dépôt et à la diffusion de documents scientifiques de niveau recherche, publiés ou non, émanant des établissements d'enseignement et de recherche français ou étrangers, des laboratoires publics ou privés.

## Retrieval of average CO<sub>2</sub> fluxes by combining in situ CO<sub>2</sub> measurements and backscatter lidar information

Fabien Gibert,<sup>1</sup> Martina Schmidt,<sup>2</sup> Juan Cuesta,<sup>1</sup> Philippe Ciais,<sup>2</sup> Michel Ramonet,<sup>2</sup> Irène Xueref,<sup>2</sup> Eric Larmanou,<sup>3</sup> and Pierre Henri Flamant<sup>1</sup>

Received 27 October 2006; accepted 1 February 2007; published 16 May 2007.

[1] The present paper deals with a boundary layer budgeting method which makes use of observations from various in situ and remote sensing instruments to infer regional average net ecosystem exchange (NEE) of CO<sub>2</sub>. Measurements of CO<sub>2</sub> within and above the atmospheric boundary layer (ABL) by in situ sensors, in conjunction with a precise knowledge of the change in ABL height by lidar and radiosoundings, enable to infer diurnal and seasonal NEE variations. Near-ground in situ CO measurements are used to discriminate natural and anthropogenic contributions of CO<sub>2</sub> diurnal variations in the ABL. The method yields mean NEE that amounts to  $5 \mu\text{mol m}^{-2} \text{s}^{-1}$  during the night and  $-20 \mu\text{mol m}^{-2} \text{s}^{-1}$  in the middle of the day between May and July. A good agreement is found with the expected NEE accounting for a mixed wheat field and forest area during winter season, representative of the mesoscale ecosystems in the Paris area according to the trajectory of an air column crossing the landscape. Daytime NEE is seen to follow the vegetation growth and the change in the ratio diffuse/direct radiation. The CO<sub>2</sub> vertical mixing flux during the rise of the atmospheric boundary layer is also estimated and seems to be the main cause of the large decrease of CO<sub>2</sub> mixing ratio in the morning. The outcomes on CO<sub>2</sub> flux estimate are compared to eddy-covariance measurements on a barley field. The importance of various sources of error and uncertainty on the retrieval is discussed. These errors are estimated to be less than 15%; the main error resulted from anthropogenic emissions.

**Citation:** Gibert, F., M. Schmidt, J. Cuesta, P. Ciais, M. Ramonet, I. Xueref, E. Larmanou, and P. H. Flamant (2007), Retrieval of average CO<sub>2</sub> fluxes by combining in situ CO<sub>2</sub> measurements and backscatter lidar information, *J. Geophys. Res.*, 112, D10301, doi:10.1029/2006JD008190.

### 1. Introduction

[3] Ecosystem carbon exchanges on spatial scales of approximately 1 km<sup>2</sup> can be well documented using the eddy-covariance (EC) technique [e.g., *Wofsy et al.*, 1993; *Baldocchi et al.*, 1996; *Valentini et al.*, 2000]. However, a few data exist on the carbon budget at the regional scale, ranging from a few tenths to a few hundreds of square kilometers. At these scales, the carbon fluxes can be estimated either by upscaling pointwise flux measurements using for instance airborne flux transects, biophysical models, and remote sensing information [*Turner et al.*, 2004, *Miglietta et al.*, 2006] or by inverting atmospheric concentration measurements using a fine-scale mesoscale transport model (M. Uliasz, et al., Uncovering the lake

signature in CO<sub>2</sub> observations at the WELF tall tower: A modelling approach, submitted to *Agricultural and Forest Meteorology*, 2006). This latter method however is still under development and requires very dense atmospheric observation data sets (A. J. Dolman, et al., CERES: The CarboEurope Regional Experiment Strategy in Les Landes, South West France, May–June 2005, submitted to *Bulletin of the American Meteorological Society*, 2006).

[4] In the near future, passive remote sensing instruments will be launched soon (OCO, GOSAT) [*Crisp et al.*, 2004; *Inoue*, 2005] to measure column CO<sub>2</sub> concentration and to constrain regional flux inversions. In this context, a differential absorption lidar (DIAL) has been developed at the Institut Pierre Simon Laplace (IPSL)-Laboratoire de Météorologie Dynamique (LMD) to conduct simultaneous measurements on CO<sub>2</sub> density and atmospheric boundary layer (ABL) structure [*Gibert et al.*, 2006]. The two sets of measurements provide information on CO<sub>2</sub> reservoirs and mixing processes during the diurnal cycle.

[5] The goal of this paper is to infer surface CO<sub>2</sub> fluxes at larger scale than EC measurements by estimating the processes that control the CO<sub>2</sub> concentration variations in the atmospheric boundary layer (ABL). Several analyses of the CO<sub>2</sub> mass balance of the ABL have already been reported to

<sup>1</sup>Institut Pierre Simon Laplace, Laboratoire de Météorologie Dynamique, Ecole Polytechnique, Palaiseau, Cedex, France.

<sup>2</sup>Institut Pierre Simon Laplace, Laboratoire des Sciences du Climat et de l'Environnement, UMR CEA/CNRS 1572, Gif-sur-Yvette, Cedex, France.

<sup>3</sup>INRA Unité Mixte de Recherche INRA/INAPG "Environnement et Grandes Cultures", Thiverval-Grignon, France.

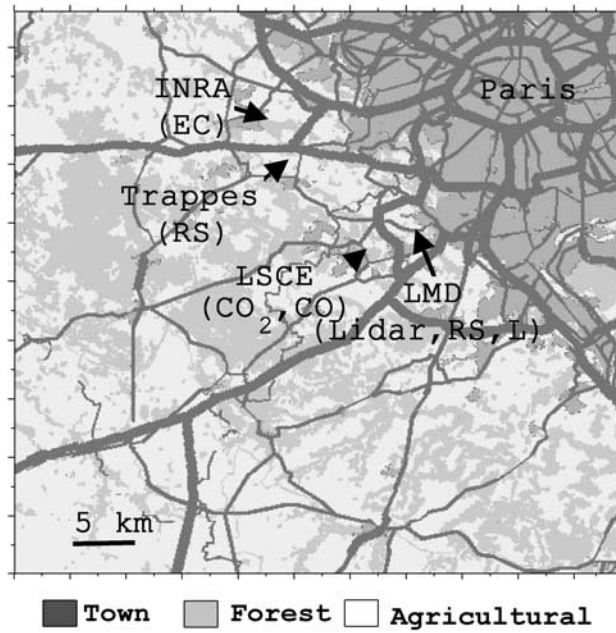


**Figure 1.** Measurement area with CO<sub>2</sub> and CO in situ ground-based measurements at LSCE laboratory. Lidar and pyranometer (*L*) measurements at LMD laboratory and radiosoundings (*RS*) at Trappes and LMD facilities. Eddy-covariance (*EC*) system to measure CO<sub>2</sub> flux above crops at INRA facility.

estimate regional-scale fluxes, usually with aircraft vertical profiles [Levy *et al.*, 1999; Lloyd *et al.*, 2001]. These studies stressed that accurate estimates of the ABL height, structure, and evolution and information on horizontal advection are essential to determine the surface fluxes. In most cases, the ABL budgets were measured only during the day, and the lack of nighttime information is problematic to estimate respiration sources [Lloyd *et al.*, 2001].

[6] Elastic scatter lidar has already showed its abilities to monitor the diurnal cycle of the ABL [Menut *et al.*, 1999]. In this paper, a new ABL mass balance method is developed to retrieve land biotic regional fluxes of CO<sub>2</sub> in the southwest of Paris during one growing season. The study covers March through September 2004, when the land biotic fluxes dominate anthropogenic emissions in controlling CO<sub>2</sub> variations in the ABL. The method uses ground-level in situ continuous CO<sub>2</sub> observations, airborne CO<sub>2</sub> vertical profiles reaching into the free atmosphere, radiosoundings, and lidar measurements (Figure 1). Solar flux pyranometer measurements are also used. We seek to provide separate estimates of the nighttime and daytime regional mean net ecosystem exchange (*NEE*) and of the flux of CO<sub>2</sub> due to entrainment at the top of the ABL (*M*). The regional *NEE* inferred from ABL observations is compared with *EC* flux measurements conducted over a barley field.

## 2. Processes That Drive CO<sub>2</sub> Variations in the Boundary Layer

### 2.1. CO<sub>2</sub> Balance in the ABL

[7] The mean CO<sub>2</sub> mixing ratio in the ABL changes in response to land biotic fluxes, dynamical processes, and

anthropogenic emissions. A mass balance approach shows that the rate of change in the CO<sub>2</sub> mean mixing ratio in the ABL,  $\langle C \rangle$ , is driven by the sum of the fluxes across the boundaries of an air column extending from the ground to the top of the layer considered. Accordingly, the evolution of  $\langle C \rangle$  is described by the following equation [Lloyd *et al.*, 2001; Gerbig *et al.*, 2003]:

$$\rho h \frac{d\langle C \rangle}{dt} = NEE + M + A \quad (1)$$

where  $\rho$  is the mean molar air density (mole per cubic meter),  $h$  is the ABL height (meter),  $C(z, t)$  is the mixing ratio profile of CO<sub>2</sub> in the ABL, *NEE* is the mean regional net ecosystem exchange (mole per square meter per second), and *M* is the molar flux per surface unit due to vertical mixing with the upper layer, either the residual layer (*RL*) or the free atmosphere (*FA*). *NEE* is representative of the heterogeneously distributed fluxes that are transported by mesoscale flow. We consider that the ABL spatially integrates surface fluxes over areas with length scales much larger than  $h$  [Gloor *et al.*, 1999]. *A* is the flux of CO<sub>2</sub> from advected anthropogenic emissions.

[8] The value of  $\langle C \rangle$  and *M* are given by:

$$\langle C(t) \rangle = \frac{1}{h} \int_0^h C(z, t) dz \quad (2)$$

$$M = \rho \frac{dh}{dt} (C_+ - \langle C \rangle) \quad (3)$$

where  $C_+$  is the CO<sub>2</sub> mixing ratio in the layer above the ABL. The term  $dh/dt$  accounts for the vertical velocity induced by large-scale atmospheric motion as subsidence and by the ABL growth and decay controlled by sensible heat flux. In other studies [Lloyd *et al.*, 2001; Gerbig *et al.*, 2003], subsidence has been added explicitly in equation (3). Here we included it in equation (3) because of the nature of our  $h$  observations (section 4.2).

[9] Daytime *NEE*<sub>day</sub> is assumed to decrease linearly with the total short-wave solar flux (see section 6):

$$NEE_{day} = -\alpha L + \beta \quad (4)$$

where *L* is the total (direct + diffuse) short-wave downwelling solar flux (watt per square meter) measured by a pyranometer, and  $\beta$  is the *NEE* value at the sunrise. We call  $\alpha$  the light conversion factor which reflects biological processes (micromole per square meter per second/watt per square meter).

### 2.2. Characteristic Diurnal Regimes

[10] Figure 2 shows typical summertime diurnal variations of CO<sub>2</sub> measured near the ground using a gas chromatograph and of the ABL thickness  $h$  measured from elastic backscatter lidar measurements, together with the solar flux from pyranometer measurements (see section 3). Three distinct regimes can be seen.

[11] 1. During the night, the CO<sub>2</sub> mixing ratio usually increases linearly from 2000 to 0500 UT. The nocturnal boundary layer (*NBL*) behaves as a reservoir filled with the nocturnal plant and soil respiration emissions. Assuming

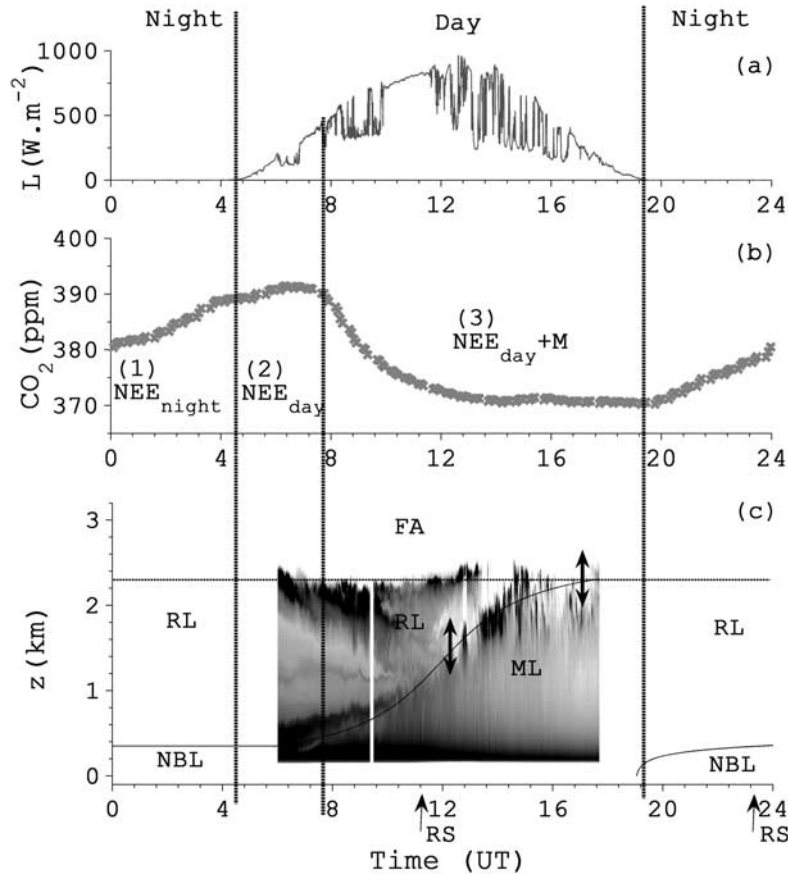


**Figure 2.** 30 July 2004: (a) Pyranometer solar flux measurements. (b) CO<sub>2</sub> ground-based in situ measurements at 10 m height (IPSL/LSCE). Biological and dynamical processes that govern CO<sub>2</sub> diurnal cycle have been added: *NEE*, net ecosystem exchange; *M*, mixing. (c) Lidar 532-nm boundary layer aerosol backscatter signal. The boundary layer diurnal cycle is also represented: RL, residual layer; NBL, nocturnal boundary layer; ML, mixed layer; FA, free atmosphere [Stull, 1988]. The double arrows indicate the vertical mixing with, first, the RL and, second, the FA. The simple arrows are for the daily Trappes radiosoundings (RS).

anthropogenic emissions to cause only a weak disturbance from the respiration-driven linear increase of CO<sub>2</sub> (see section 4.1) and knowing the NBL height ( $h_{NBL}$ ), the nighttime NEE flux is given by:

$$NEE_{night} = \rho h_{NBL} \frac{d\langle C \rangle}{dt} \quad (5)$$

[12] 2. Between the sunrise and the occurrence of the mixed layer (ML) at 0800 UT, both respiration and photosynthesis influence the rate of change of near-ground CO<sub>2</sub>. At this time of the day, a strong temperature inversion often remains from the former night, which is not disturbed by solar heating ( $L < 500 \text{ W m}^{-2}$ ). Therefore, assuming that  $h = h_{NBL}$  during this morning regime, the daytime  $NEE_{day}$  is also given by equation (5).

[13] 3. Between approximately 0800 and 1400 UT, the near-ground CO<sub>2</sub> mixing ratio is decreasing due to photosynthesis and vertical mixing with the residual layer (RL) and eventually the free atmosphere (FA) above (see arrows in Figure 2c). The CO<sub>2</sub> mixing ratio is well mixed inside the convective boundary layer. At the end of the afternoon, the near-ground CO<sub>2</sub>

mixing ratio becomes nearly equal to the value in the free troposphere. All fluxes in equation (1) are active. However, as the ML is more than 1000 meters thick, the surface fluxes change the CO<sub>2</sub> mixing ratio only slowly with time.

### 2.3. Contamination by Anthropogenic Emissions

[14] The measurement sites are located 20 km at southwest of Paris in a rural area (Figure 1). Figure 3 displays the average near-ground CO<sub>2</sub> and CO diurnal cycles observed between April and September, together with the mean road traffic index in Paris urban area (SYTADIN data are available at <http://www.sytadin.equipement.gouv.fr>). Car traffic accounts for ~60% of the Paris CO<sub>2</sub> emissions during that period (CITEPA and AIRPARIF data are available at <http://citepa.org> and <http://www.airparif.asso.fr>, respectively). Therefore CO can be used as a car traffic marker to evaluate the anthropogenic contamination of the CO<sub>2</sub> diurnal variations. Depending on the wind direction, an increase in the CO<sub>2</sub> mixing ratio is expected during the rush hours between 0600 and 0800 UT in the morning (or 0800 and 1000 UT local summertime) and between 1600 and 1800 UT in the evening. The effect of emissions on ABL CO<sub>2</sub> mixing ratios

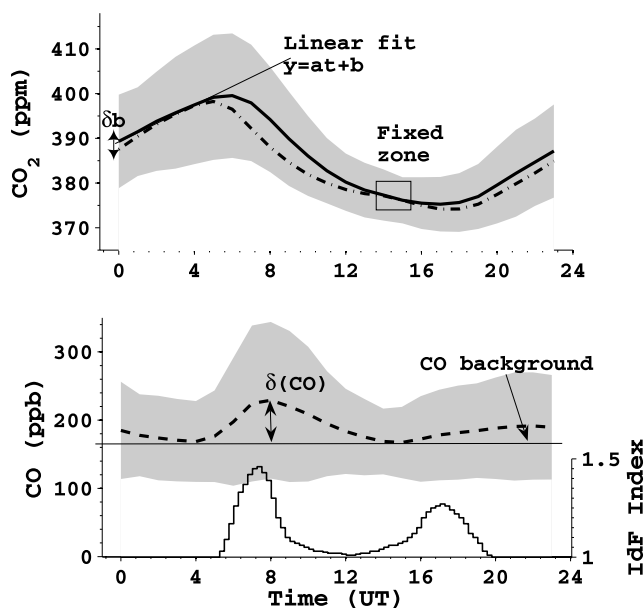


**Figure 3.** Mean ground-based CO<sub>2</sub> (solid line) and CO (dashed line) in situ measurements between April and September 2004. The time resolution is 5 min. The grey areas correspond to the standard deviation. The mean anthropogenic CO<sub>2</sub> is calculated using CO measurements (assuming that 10 ppb of CO corresponds to 1 ppm of anthropogenic CO<sub>2</sub>, i.e.,  $\eta = 0.1$ ) and then is deducted from the whole CO<sub>2</sub> diurnal cycle to retrieve the CO<sub>2</sub> natural variations (dashed and dotted line). The “fixed zone” considered to constrain regional flux retrieval is indicated as a rectangle and corresponds to  $\sim 20$  points or 2 hours of CO<sub>2</sub> measurements in the mid-afternoon. Linear fit  $y = at + b$  is used to retrieve the respiration flux during the night. The mean road traffic index in Paris urban area during this period of time is also displayed (SYTADIN data are available at <http://www.sytadin.equipement.gouv.fr>).

is stronger in the morning when the ABL is shallow. Braud *et al.* [2004] have shown that the anthropogenic emissions of Paris are characterized by a mean ratio CO<sub>2</sub>/CO of 0.09 (11 ppb of CO per parts per million of fossil CO<sub>2</sub>). This mean emission flux ratio should only be used as an approximation for the actual ratio of fossil CO<sub>2</sub> to CO in the atmosphere which depends on the distance between the measurement site and the diverse combustion sources as well as on local atmospheric transport. When using the fossil CO<sub>2</sub> to CO emission ratio as qualitative indication of the amount of fossil CO<sub>2</sub> in the ABL, we found that the diurnal cycle of CO<sub>2</sub> is often contaminated by urban emissions between 0700 and 1200 UT while it is rather insensitive to them in the middle of the afternoon. This “fixed zone” corresponds to approximately 2 hours or  $\sim 20$  CO<sub>2</sub> measurements (Figure 3).

### 3. Experimental Set up

#### 3.1. Study Area and Measurement Sites

[15] Twenty-one days has been analyzed to infer surface fluxes. Figure 1 shows the Paris urban area and the measurement sites, placed 20 km southwest of the most densely populated area. Quasi-continuous CO<sub>2</sub> and CO near-ground

in situ measurements are made at the IPSL-LSCE site. Solar flux and lidar measurements are made at the IPSL-LMD site, distant of LSCE from 5 km. A pyranometer at IPSL-LMD provides total ( $L$ ), direct, and diffuse solar flux observations. Meteorological sensors are in place at both sites. Vertical profiles of humidity, temperature, and horizontal wind speed are obtained from daily radiosoundings at Trappes (Figure 1) at 1100 and 2300 UT. The Trappes meteorological facility is located  $\sim 10$  km to the west of the LSCE and LMD laboratories. At such a distance in the Paris plains, terrain-induced inhomogeneities are not expected to have a major impact on the mean ABL structure and parameters. Additional radiosoundings at IPSL-LMD made during May and June 2004 confirmed this hypothesis (see section 7).

#### 3.2. CO<sub>2</sub> and CO In Situ Measurements

[16] An automated gas chromatographic system (HP-6890) was routinely operated at IPSL-LSCE for CO, CO<sub>2</sub>, CH<sub>4</sub>, N<sub>2</sub>O, and SF<sub>6</sub> semicontinuous measurements of ambient air [Worthy *et al.*, 1998]. The precision on CO<sub>2</sub> is  $\pm 0.5$  ppm with a measurement time step of 5 min [Pépin *et al.*, 2002] as shown in Figure 4. Additionally, airborne vertical CO<sub>2</sub> profiles have been conducted once every 15 days using flask sampling and a continuous LICOR NDIR gas analyzer onboard a light aircraft. These routine flights are made over the Orleans forest (80 km south of the study area). They reach up to 3000 meters, piercing the top of the ABL and sampling the lowermost free atmosphere (Figure 4).

#### 3.3. Ecosystem CO<sub>2</sub> Fluxes

[17] Eddy-covariance NEE fluxes were measured 10 km away from the IPSL-LMD and IPSL-LSCE sites above a barley canopy (INRA data are available at <http://www.inra.fr>) since May 2004. The barley winter crops were growing at that time and gradually dried up afterward until harvest took place on 2 July. After harvest, the measurements went on above a thatch field up until September.

#### 3.4. Lidar Measurements of ABL Structure

[18] Elastic lidars pointing at zenith are used to monitor the ABL structure and diurnal changes. Aerosol particles are reliable tracers of the ABL height and fluctuation. The range resolution is 15 m, and a profile is acquired every 10 s (Table 1). The ML and RL layers are respectively identified by their large and small aerosol concentrations (Figure 2). The lidar configuration precludes measurements below 200 m due to a lack of overlap between the laser transmitter and the telescope receiver. Therefore we use vertical profiles of potential temperature from Trappes radiosoundings to determine the NBL height. During the day, both lidar and radiosounding observations are used to retrieve the height of the ML.

### 4. Flux Retrieval Method

#### 4.1. Retrieval of CO<sub>2</sub> Fluxes

[19] Figure 5 shows how the different data sets were used to retrieve NEE and the ABL entrainment flux  $M$ . The value of  $M$  is determined by combining measurements of  $dh/dt$  (see section 4.2) with near-ground CO<sub>2</sub> concentrations and airborne flask CO<sub>2</sub> samples in the free atmosphere. The CO<sub>2</sub> mixing ratio in the RL is assumed to be equal to that of the ML at the end of the afternoon of the previous day (obtained by near-ground in situ data). The free tropospheric CO<sub>2</sub>

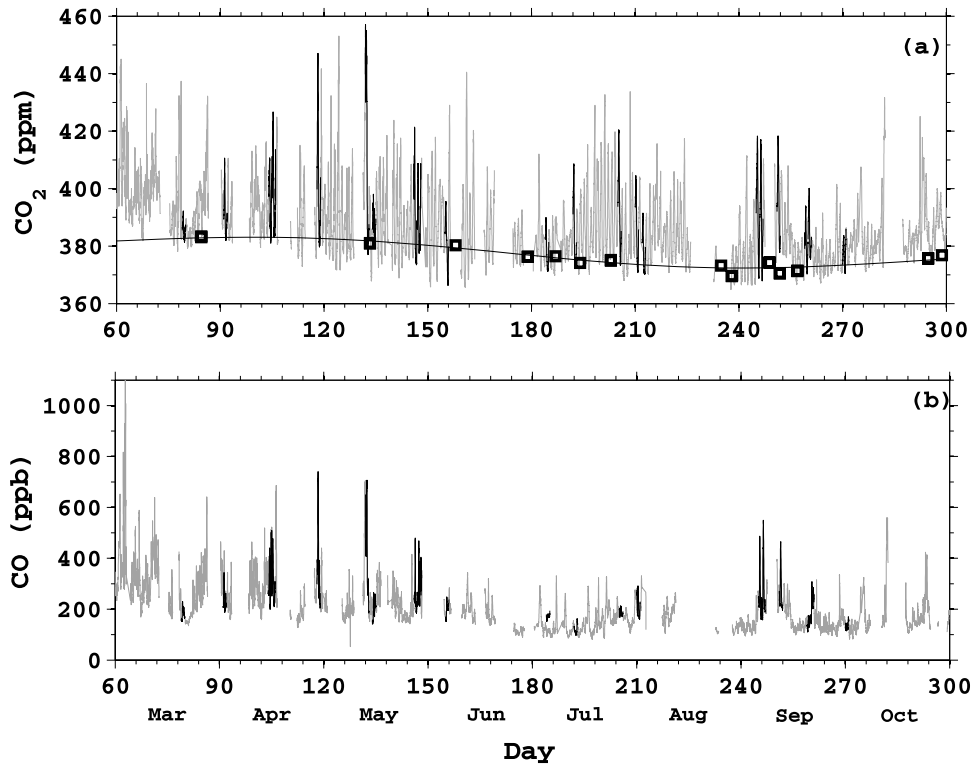


**Figure 4.** (a) CO<sub>2</sub> in situ ground-based measurements at LSCE facility (gray solid line) and free tropospheric airborne measurements 100 km south of Paris for the year 2004 [squares for each measurement and interpolation (solid line)]. (b) CO in situ ground-based measurements at LSCE facility for the year 2004 (gray solid line). The black solid lines correspond to the 21 cases studied in this paper.

value is estimated each day using a time interpolation of in situ airborne measurements (Figure 4).

[20] The NBL heights are determined from radiosoundings at 2300 (UT). Combined with hourly near-ground CO<sub>2</sub> data, the NBL height is used to determine  $NEE_{night}$  using equations (2) and (5). Figure 3 shows that, on average, the linear increase of CO<sub>2</sub> during the night implied by  $NEE_{night}$  is only weakly disturbed by anthropogenic sources. This is due both to the prevalence of well-mixed boundary layers in the late afternoon and to the very small CO<sub>2</sub> emissions at night. Fitting a linear trend to the CO<sub>2</sub> mixing ratio ( $y = at + b$ ) thus is possible and allows to infer  $NEE_{night}$ . The accounted for remaining anthropogenic emissions create statistical errors in the retrieval of  $a$  and  $b$  and add a systematic bias on the CO<sub>2</sub> diurnal cycle ( $\delta b$ ).

#### 4.1.1. Direct Method

[21] In rare occasions when the CO<sub>2</sub> diurnal cycle is not disturbed by anthropogenic emissions, we could directly determine  $NEE_{day}$  using the full time period between the sunrise and the ABL rise using equation (5). The value of  $\alpha$  was then used to determine  $NEE_{day}$  during the rest of the day using equation (4) (see Figure 5).

#### 4.1.2. Iterative Method

[22] In the vicinity from Paris urban area, the morning period is most often disturbed by anthropogenic emissions. Consequently, we cannot use equation (5) to determine  $\alpha$  in 85% of the cases studied. Knowing  $M$  and  $\beta$  ( $NEE_{night}$  at the sunrise), we thus looked for a value of  $\alpha = (NEE_{day} - \beta)/L$  that matches best the observed CO<sub>2</sub> decreasing trend during the “fixed zone”, lasting for  $\sim 2$  hours in the late afternoon

(see Figure 3).  $NEE_{day}$  is determined after several iterations adjusting  $\alpha$  in order to reach the observed trend for CO<sub>2</sub> during the late afternoon. For every iteration,  $M$  gets also adjusted using the modeled natural CO<sub>2</sub> diurnal cycle in equation (3). This iterative method does not require any hypothesis about fossil CO<sub>2</sub> to CO ratios which may be very variable (section 6.4).

[23] Without anthropogenic emissions, both the direct and the iterative methods to retrieve  $NEE_{day}$  are applicable and can be compared. This comparison is performed in section 6.2. Moreover, in the iterative method, additional information on the ratio between fossil CO<sub>2</sub> and CO in the air,  $\eta$ , can be obtained from CO in situ measurements (section 6.4).

## 4.2. Retrieval of ABL Height and $\langle C \rangle$ Using Lidar Backscatter Signal and Radiosoundings

[24] The inflexion point method (IPM) [Menut et al., 1999] is used to determine the ABL height from radiosoundings (night) and lidar backscatter signal (day). Figure 6 displays the lidar backscatter signal and the radiosounding potential

**Table 1.** Elastic Scattering Lidar Characteristics at LMD Facility<sup>a</sup>

Lasers	$\lambda$ , nm	$E$ , mJ	PRF, Hz	Telescope D, cm/FOV, mrad	$\Delta R$ , m	Averaging, s
Nd:YAG	532	30	20	20/3	15	10
	1064	15				

<sup>a</sup> $\lambda$  is the emission wavelength,  $E$  is the average output laser energy,  $D$  is the telescope diameter, FOV is the field of view, and  $\Delta R$  is the vertical resolution.

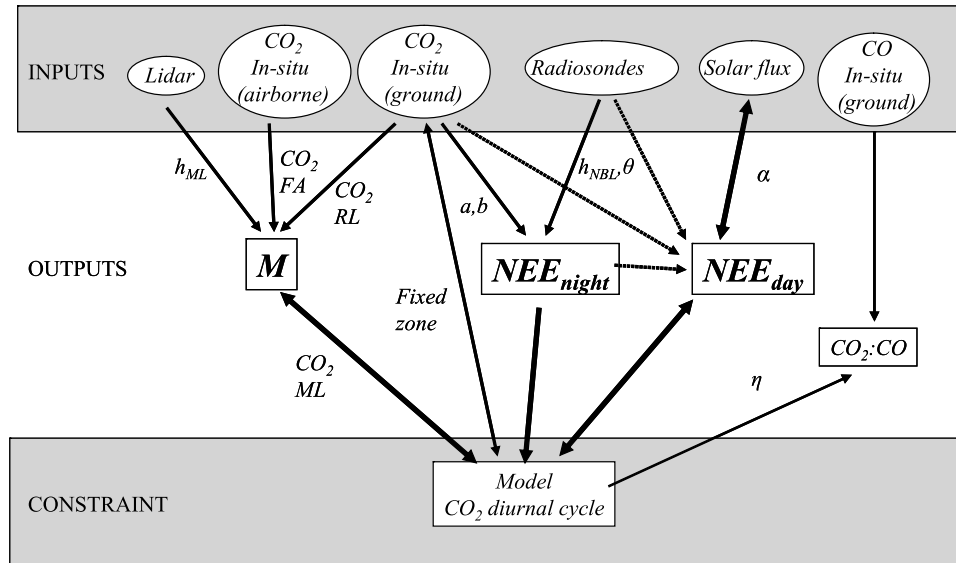


**Figure 5.** Block diagram and method to retrieve CO<sub>2</sub> surface fluxes due to biological ( $NEE$ ) and dynamical ( $M$ ) processes. Circles are for the measurements while squared frameworks are for the results. The dotted arrows are used whenever the CO<sub>2</sub> diurnal cycle is not disturbed by anthropogenic emissions. The double arrows are for successive iterations and retroactions.  $h_{NBL}$  and  $h_{ML}$  are the nocturnal and the mixed-layer height, respectively,  $\theta$  is the potential temperature,  $\alpha$  is the light conversion factor,  $a$  and  $b$  are the linear fit coefficients described in Figure 3, and  $\eta$  is the ratio between fossil CO<sub>2</sub> and CO.

temperature profiles from Trappes and LMD on 25–26 May. The 0157 UT potential temperature profile shows a large temperature inversion close to the ground, which caps the shallow NBL. This NBL height is determined from the maximum of the second-order derivative of  $\theta$ . The same method is used to determine the top of the RL.

[25] During the night, knowledge of the  $\theta$  vertical profile is usually sufficient to characterize vertical stratification and scalar gradients in the boundary layer [Stull, 1988]. Studies of CO<sub>2</sub> and H<sub>2</sub>O vertical profiles show that mixing ratios and potential temperature profiles usually have a similar shape due to nocturnal static stability [Bakwin *et al.*, 2003; Lloyd *et al.*, 2001; de Arellano *et al.*, 2004; Dolman *et al.*, 2005]. In order to determine the mean CO<sub>2</sub> mixing ratio in the NBL, we assume a similarity between the vertical gradients of  $C$  and  $\theta$ , the gradient of  $\theta$  being assumed to be constant during the whole night. This yields:

$$C(z, t) = C_{RL} + [C(0, t) - C_{RL}] \left[ \frac{\theta(0) - \theta(z)}{\theta(0) - \theta(h_{NBL})} \right] \quad (6)$$

where  $C_{RL}$  is the CO<sub>2</sub> density in the residual layer ( $h_{NBL} < z < h_{RL}$ ), and  $C(0, t)$  is the observed near-ground CO<sub>2</sub> mixing ratio. The mean CO<sub>2</sub> mixing ratio in the NBL  $\langle C \rangle$  is then obtained by solving equations (2) and (6). Errors associated to the similarity hypothesis will be analyzed in section 7.2.

[26] During the day, when the ABL is mixed by convection (Figure 2), CO<sub>2</sub> can be assumed to be constant vertically and equal to the near-ground in situ value. Thus  $\langle C \rangle = C(0, t)$ . The convective ABL height is determined by the inflexion point method minimizing the second derivative of backscatter lidar signal with respect to altitude  $\partial^2(Pz^2)/\partial z^2$ . The mixed-layer height  $h_{ML}$  is then defined as the middle of the transition zone between the mixed layer

and the free troposphere (see Figure 6). The ML heights determined either from the lidar signals or from radiosounding profiles are comparable within 5%.

## 5. Results

### 5.1. Diurnal Trends Controlling CO<sub>2</sub> in the ABL

[27] The inferred NEE and mixing CO<sub>2</sub> fluxes are shown in Figure 6c for the period 25–26 May. The flux  $M$  is the largest for a maximum difference in CO<sub>2</sub> mixing ratio between ML and RL and when the ABL rate of growth is maximal. During the growth of the ABL, thermal overshoots entrain air from, first, the residual layer and, second, from the free atmosphere. This entails a significant dilution of the ABL concentrations in trace gases. Thus mixing combined with daytime NEE uptake causes a large drop of CO<sub>2</sub> in the morning. Remark that CO<sub>2</sub> is decreased much more effectively by vertical mixing than by NEE during the morning growth of the ABL, as also observed by Yi *et al.* [2000], Davis *et al.* [2003], and de Arellano *et al.* [2004]. In the afternoon, NEE persistently removes CO<sub>2</sub> from the ABL but results only into a small trend of the mixing ratio value (−1.1 ppm/hr) because the height of the ABL is maximum. The case of 26 May is not ideal because a rainfall occurred at 1600 UT with dense clouds reducing the NEE uptake of CO<sub>2</sub> (Figures 6a and 6c). During the afternoon well-mixed ABL regime, it is worth noting that  $M$  is slightly positive (see, for example, Figure 6c for 25 May and Figure 7 for 27 April), meaning that CO<sub>2</sub> enters from the free troposphere into the boundary layer.

[28] Once the NEE parameters ( $NEE_{night}$  and  $\alpha$ ) are determined, we can model the full diurnal variation of CO<sub>2</sub> (caused by biotic fluxes only) in the ABL. For the “clean days”, without anthropogenic emissions, the modeled drop of land biotic CO<sub>2</sub> in the morning is in good agreement with

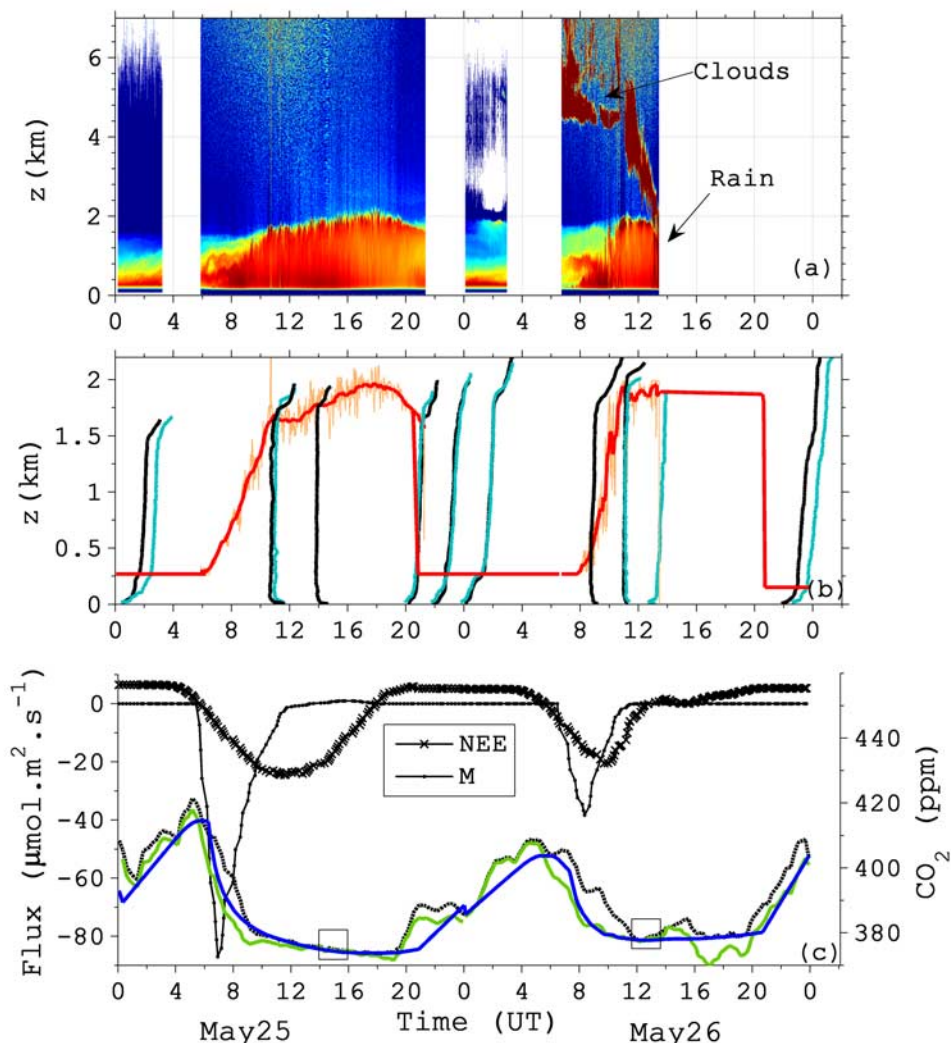


**Figure 6.** 25 and 26 May 2004: (a) Backscatter lidar signal. Color plot is for  $\ln(Pz^2)$  in arbitrary unit (red is for higher return signal). (b) NBL and ML height retrievals from the inflexion point method (IPM). The ABL height is displayed using backscatter lidar measurements (fine solid line) and is smoothed to retrieve the mean ABL height (bold red solid line). Potential temperature profiles from radiosoundings, launched at LMD (black solid line) and at Trappes (blue solid line) facilities, are displayed in arbitrary units. These profiles are used to calculate the mean NBL height. (c) Flux retrievals.  $NEE$  is the net ecosystem exchange from the respiration and the photosynthesis uptake, and  $M$  is the flux due to the vertical mixing. Total CO<sub>2</sub> mixing ratio from in situ measurements (black dashed line) and land biotic CO<sub>2</sub> (obtained using a linear correction by CO measurements) (green solid line) and modeled CO<sub>2</sub> diurnal cycles (blue solid line) are also displayed. The rectangles correspond to the fixed zones used to compute the modeled natural CO<sub>2</sub> diurnal cycle.

the observations, which validates our assumptions of homogeneous mixing of regional fluxes and  $NEE_{day}$  being proportional to solar radiation (19 March and 30 July in Figure 7). For the “polluted days”, on the other hand, an extra fossil CO<sub>2</sub> component is needed in the ABL budget to fit the morning CO<sub>2</sub> drop (27 April and 1 September in Figure 7).

## 5.2. Seasonal Variations

[29] The results are given in Figure 8. The seasonal evolution of the flux  $M$  reflects seasonal variations in the ABL rate being linked to the stratification of the ABL during the night (strength of temperature inversion) and to the

turbulent energy transfer with the air above [Stull, 1988]. A seasonal maximum in  $M$  amplitude can be seen in the middle of the year when the surface sensible heat flux reaches a maximum (see  $M_{min}$  values in Figure 8a and  $H$  values in Figure 8b). In summer, the flux  $M$  is a sink for CO<sub>2</sub> in the ABL during the morning and a source during the afternoon, when the tropospheric CO<sub>2</sub> value is higher than the ML one, due to vegetation uptake. More precisely, Figure 8a shows that  $M$  is a net daily source of CO<sub>2</sub> for the ABL in May, when CO<sub>2</sub> value remains higher in the free troposphere than in the ABL [see also de Arellano et al., 2004; Yi et al., 2004; Bakwin et al., 2004; Hellinker et al., 2004].

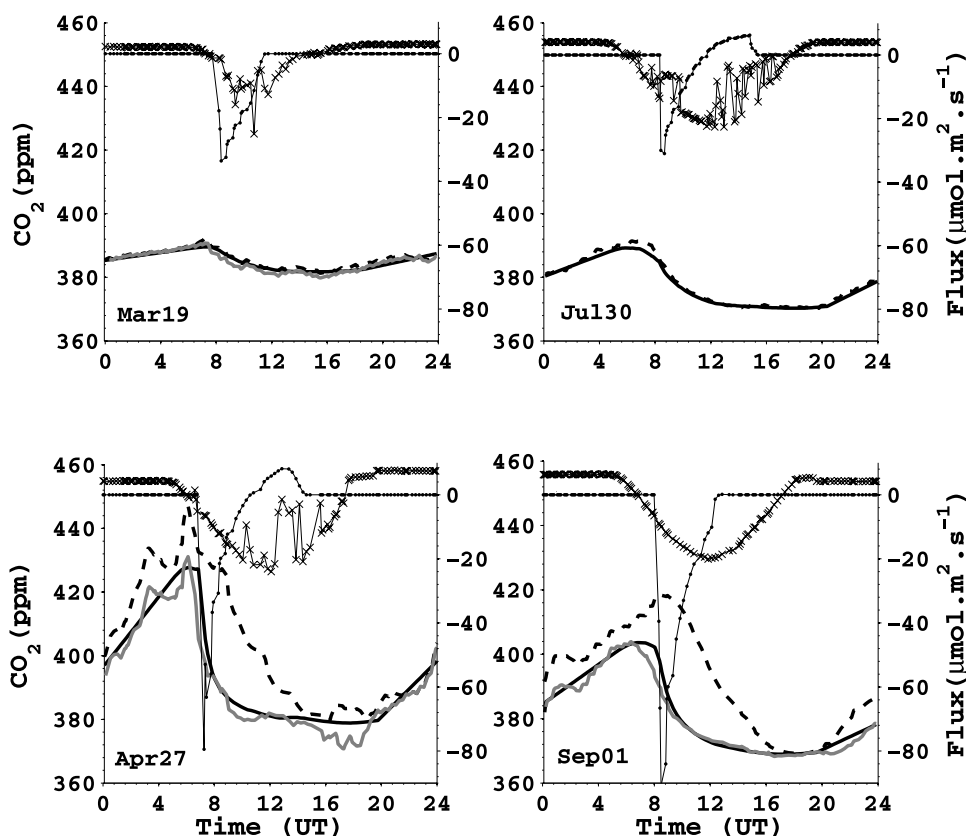


**Figure 7.** NEE and M retrievals and CO<sub>2</sub> diurnal cycle for four cases in the year 2004: 19 Mar, 27 Apr, 30 Jul, and 1 Sep. In situ CO<sub>2</sub> ground-based measurements from LSCE facility (black dashed line) and approximated CO<sub>2</sub> diurnal natural variations using a linear correction from CO measurements (grey solid line). The black solid line is for the model.

[30] Between April and June, both daytime and nighttime NEE amplitudes reach their seasonal maximum (Figure 8a) in good agreement with the local growing season and with the eddy-covariance measurements above forests and crops in western Europe [Granier *et al.*, 2002; Perrin *et al.*, 2004; Moureaux *et al.*, 2006]. Day-to-day variations in NEE are further investigated in sections 6.2 and 6.3.

[31] The standard deviation and the mean difference between modeled ( $C_m$ ) and observed ( $C_e$ ) daily CO<sub>2</sub> mixing ratios are displayed in Figure 8c. Even for polluted days associated with high levels of CO (27 April, 11 May, and 1–2 September), the modeled diurnal fluctuation of land biotic CO<sub>2</sub> is in good general agreement with the in situ data corrected for anthropogenic effects ( $C_e - \eta\delta(\text{CO})$ ). The mean difference of the means  $\langle C_e - \eta\delta(\text{CO}) - C_m \rangle$  equals  $-0.6$  ppm, and the mean standard deviation between the model and the corrected data  $\sigma(C_e - \eta\delta(\text{CO}) - C_m)$  is 2.1 ppm. For the clean days less contaminated by anthropogenic sources (19 March, 2 July, 30 July, and 26 September), the model produces its best agreement with the data, and the mean standard deviation is below 1 ppm.

## 6. Discussion

### 6.1. Comparison With Eddy-Covariance Fluxes Measurements

[32] In the region study, agriculture (mainly winter wheat) represents 50% of the land use while forests (mostly oaks) cover 30% (CHAMBAGRI and IFN data are available at

<http://www.ile-de-france.chambagri.fr> and <http://www.ifn.fr>, respectively), the rest being urban. Crops usually have higher daytime NEE uptake rates than forests, but their growing season is shorter. We compared the inferred regional NEE to the Barley eddy-covariance data (see section 3.3) in Figure 8d. The eddy-covariance NEE exhibits the highest photosynthesis rates in mid-May and lower values afterward when the plants begin to dry. After harvest on 2 July, the thatch field releases CO<sub>2</sub> into the atmosphere.

[33] The scales at which ABL budgeting and eddy-covariance methods measure NEE are so different that a direct comparison is not feasible. However, we can look for similarities in seasonal and synoptic NEE changes even if we expect different values. The ABL-inferred NEE has a quite different phase than eddy-covariance data. The regional NEE keeps negative values after the harvest and is therefore influenced by other ecosystems than just winter cereal fields. A zoom on the 25–26 May period (Figure 8d) compares ABL and eddy-covariance NEE. The daytime values are nearly the same (except for 26 May maybe because of cloudiness differences). The nighttime respiration values are markedly higher in the NBL budgeting method ( $5 \mu\text{mol m}^{-2} \text{s}^{-1}$ ) compared to the flux tower measurements ( $2 \mu\text{mol m}^{-2} \text{s}^{-1}$ ) possibly because cultivated soils contain less carbon than forest soils, influencing the NBL trends. In September, a similar negative trend of nighttime NEE between NBL and eddy-covariance method

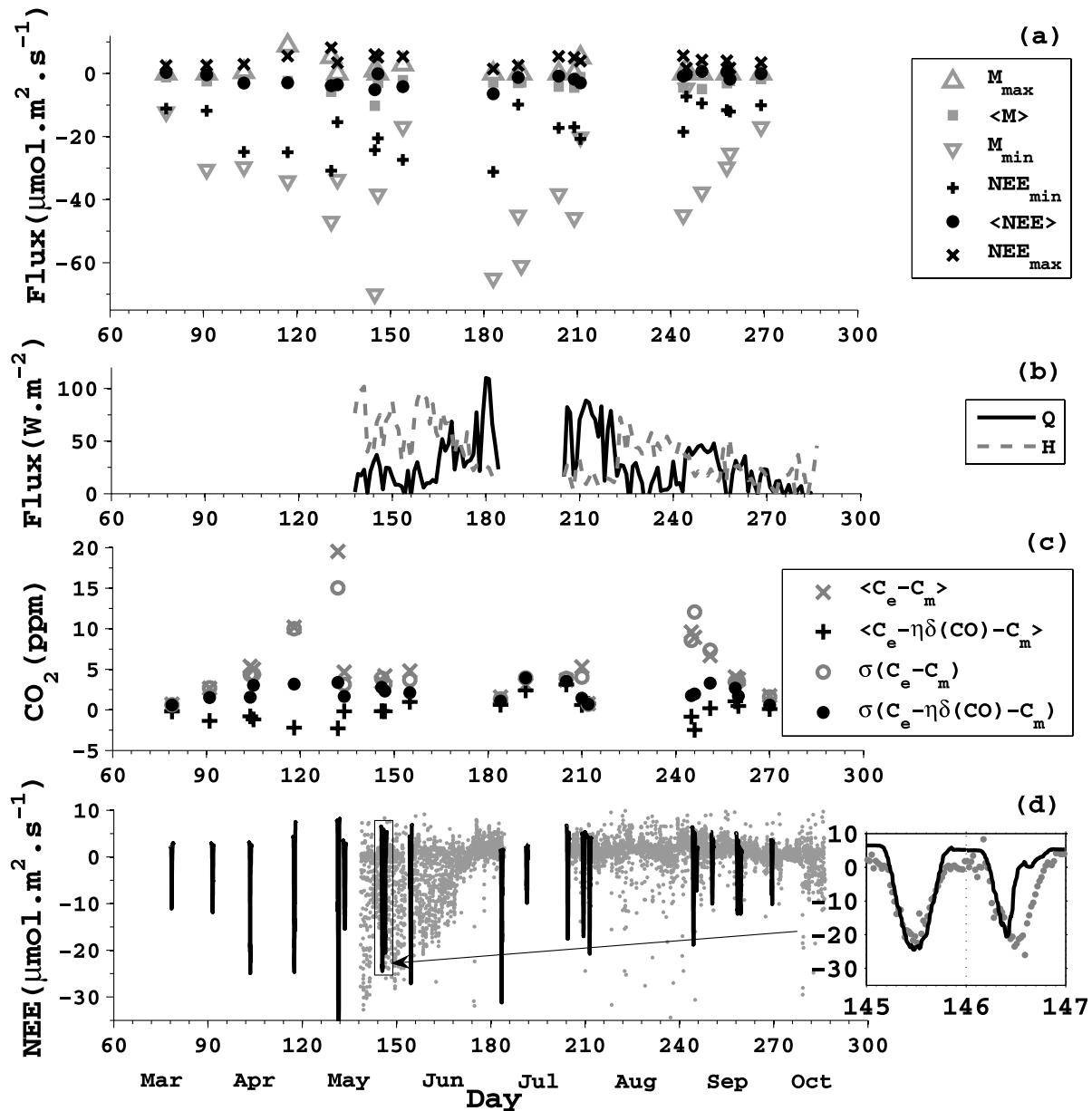


**Figure 8.** (a) Fluxes retrievals obtained for the 21 cases studied in the year 2004.  $NEE$  is the net ecosystem exchange [cross (minimum values), filled circles (mean daily values), times cross (maximum values)], and  $M$  is the flux due to the vertical mixing [empty triangles (maximal and minimal values) and filled squares (mean daily values)]. (b) Sensible  $Q$  (solid line) and latent  $H$  (dashed line) heat fluxes measured at INRA facility. (c) Difference of the mean daily  $CO_2$  mixing ratios from the ground-based measurements [ $C_e$  and  $C_e - \eta\delta(CO)$ ] and the modeled diurnal cycles ( $C_m$ ). The daily standard deviations between  $C_e$  and  $C_m$  and between  $C_m$  and  $C_e - \eta\delta(CO)$  are also displayed. (d) Inferred  $NEE$  from the boundary layer budget and measured using an eddy-covariance system above a barley field at INRA facility. INRA  $NEE$  measurements begin on 15 May. The gap in July is for the harvest period. A zoom is displayed for the two cases 25 and 26 May 2004.

can be seen. This decrease is parallel to the decrease of the heat and the latent fluxes (Figures 8b and 8d).

## 6.2. NEE Response to Solar Flux

[34] We have assumed in equation (4) that  $NEE_{day}$  increases linearly with incoming short-wave solar flux. To further test this hypothesis, we regressed the eddy-covariance  $NEE$  as a function of the solar flux in May. Even under clear-

sky conditions with high solar flux (for example, up to  $1000 \text{ W m}^{-2}$  on 25 May), the daytime  $NEE$  uptake was always observed to increase linearly with  $L$  (Figure 9a). Such a linear behavior is observed for crop canopies [e.g., *Anthoni et al.*, 2004a], but not for forests, where  $NEE$  often saturates with light [*Granier et al.*, 2002; *Anthoni et al.*, 2004b].

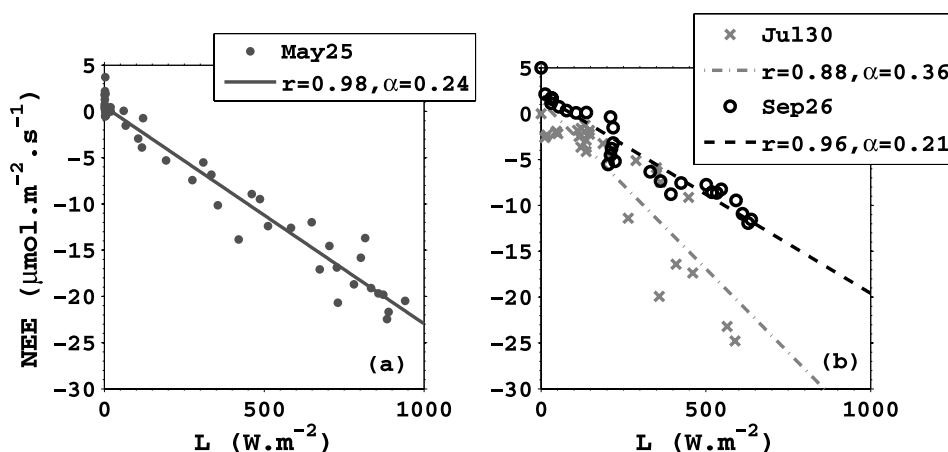


**Figure 9.** NEE as a function of the total radiative solar flux  $L$ : (a) Measured at INRA facility above a barley field on 25 May 2004; (b) estimated from equation (5) and LSCE ground-based CO<sub>2</sub> measurements in July and September during the period of time (2) (see Figure 2). The linear correlation coefficient ( $r$ ) and the absolute value of the slope ( $\alpha$ ) [ $\mu\text{mol m}^{-2} \text{s}^{-1}/(\text{W m}^{-2})$ ] are indicated.

[35] For the “clean days”, by using equation (5), we can determine directly the regional NEE dependency on solar flux for the morning period (Figure 9b). This inference is limited in time between the sunrise and the onset of convection. The days of 30 July and 26 September are best suited for this exercise, being almost exempt of anthropogenic contamination during the morning and characterized by a late onset of convection. During these 2 days, a highly significant linear relationship between NEE and  $L$  was found (the lower correlation on 30 July being due to partly cloudy conditions as seen in Figure 2).

[36] Figure 10 further shows the seasonal variation of  $\alpha$  inferred from the ABL budgeting method. A maximum is seen in May during the peak of the growing season. The error bars on  $\alpha$  reflect errors on the method and on the determination of the afternoon fixed zone. The potential contamination of the CO<sub>2</sub> trends during the afternoon fixed zone by anthropogenic emissions could also induce a systematic error on  $\alpha$ . For clean days, we can compare the “direct” and “iterative” methods to determine  $\alpha$  during the morning. The values of  $\alpha$  obtained by both methods are shown in Figure 10, showing their good agreement (mean difference of  $\pm 11\%$ ).

[37] Several studies have shown that canopy light-use efficiency (proportional to our light conversion factor  $\alpha$ ) is higher under diffuse radiation conditions [Gu *et al.*, 2002; Min, 2005]. We hence investigated the dependency of daily  $\alpha$  upon the diffuse fraction  $\phi$  of the solar flux (Figure 11a) and found a significant positive correlation between  $\alpha$  and  $\phi$  ( $r = 0.76$ ). Variations in the diffuse fraction of light were found to explain 36% of the variance of  $\alpha$  between March and July. In addition, daily variations in  $L$  are anticorrelated with  $\alpha$  ( $r = -0.62$ ) as shown in Figure 11b. Higher net solar fluxes are usually associated to clear-sky conditions (small values of  $\phi$ ) and to a decrease of the relative humidity in the ABL. Figure 11c shows that  $\alpha$  is weakly correlated with relative humidity changes ( $r = 0.36$ ), possibly suggesting effects of plant water stress.

### 6.3. Nighttime Respiration Process and Response to Air Temperature

[38] Temperature is a commonly studied environmental control on soil respiration [Lloyd and Taylor, 1994; Kätterer *et al.*, 1998; Granier *et al.*, 2002; Perrin *et al.*, 2004; Reichstein *et al.*, 2003]. Soil temperature increasingly lags air temperature deeper into the soil, but a significant positive correlation between air temperature ( $T_{\text{air}}$ ) and respiration is still observed at flux tower sites, especially between May and September when the discrepancies between air and soil temperatures are reduced [Moureaux *et al.*, 2006]. Figure 12 shows a weak correlation between our inferred respiration ( $NEE_{\text{night}}$ ) and air temperature [ $r = 0.43$ ;  $p = (0.35 \pm 0.17) \mu\text{mol m}^{-2} \text{s}^{-1}/^{\circ}\text{C}$  in Figure 12a].

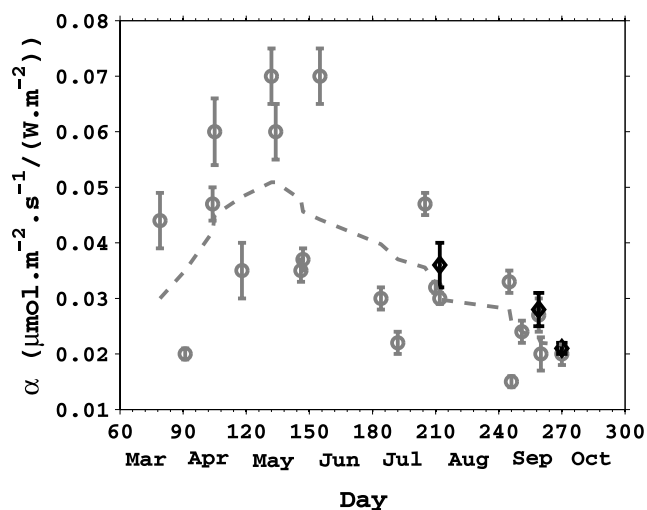


**Figure 10.** Light conversion factor,  $\alpha$  [ $\mu\text{mol m}^{-2} \text{s}^{-1}/(\text{W m}^{-2})$ ], as a function of time for the several cases studied during the year 2004 using the iterative method (grey circles) and using the direct method (Figure 5, dotted arrows) (black diamonds). A 4-point sliding averaging on  $\alpha$  estimates is also displayed (dashed line).

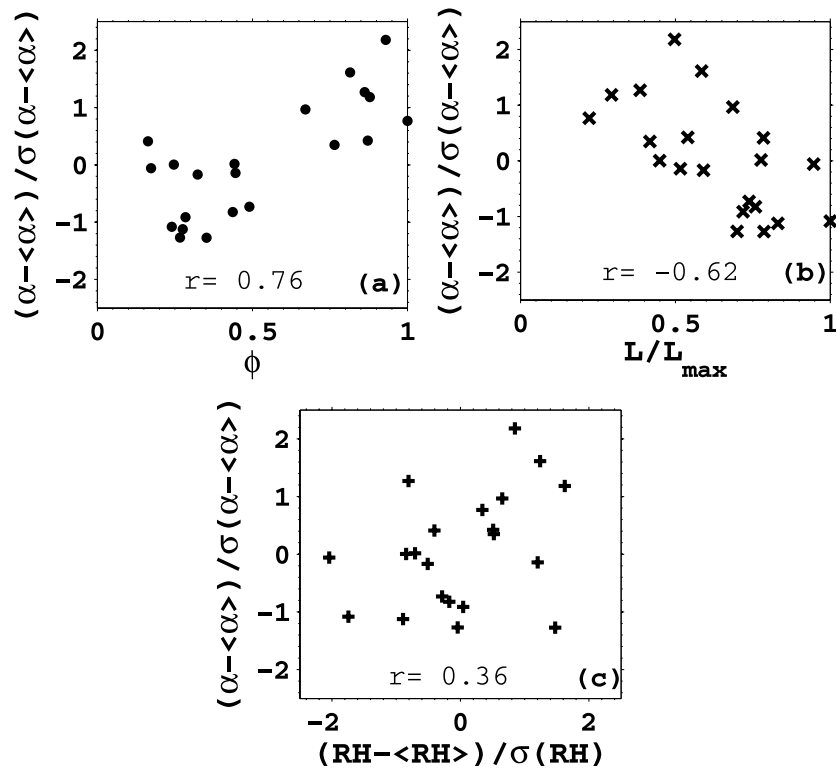


**Figure 11.** Normalized variations of the light conversion factor  $(\alpha - \langle \alpha \rangle) / \sigma(\alpha - \langle \alpha \rangle)$  as a function of (a) the proportion of diffuse irradiance  $\phi$ , (b) the normalized net irradiance  $L/L_{\max}$ , and (c) the normalized variations of the measured ground relative humidity at IPSL-LMD,  $(RH - \langle RH \rangle) / \sigma(RH)$ .

The linear slope of respiration versus  $T_{air}$  is larger in April–May than during July–September possibly because of higher soil water content in spring [Moureaux *et al.*, 2006].

#### 6.4. Estimates of Regional Fossil CO<sub>2</sub> to CO Emission Ratios

[39] We can calculate for each day the hourly fraction of land biotic CO<sub>2</sub> and can deduce by difference from the

observations the fraction of anthropogenic CO<sub>2</sub>. This makes it possible to estimate daily values of the ratio  $\eta$  of fossil CO<sub>2</sub> to CO. This ratio may vary in space and time depending on the nature and heterogeneity of anthropogenic sources (higher temperature combustions emitting less CO relative to CO<sub>2</sub>) and on the footprint of the atmospheric measurement site with respect to diverse CO and CO<sub>2</sub> sources. Fortunately, the semirural IPSL-LSCE site is far enough from immediate pollution sources. The daily values of the ratio  $\eta$ , as a function

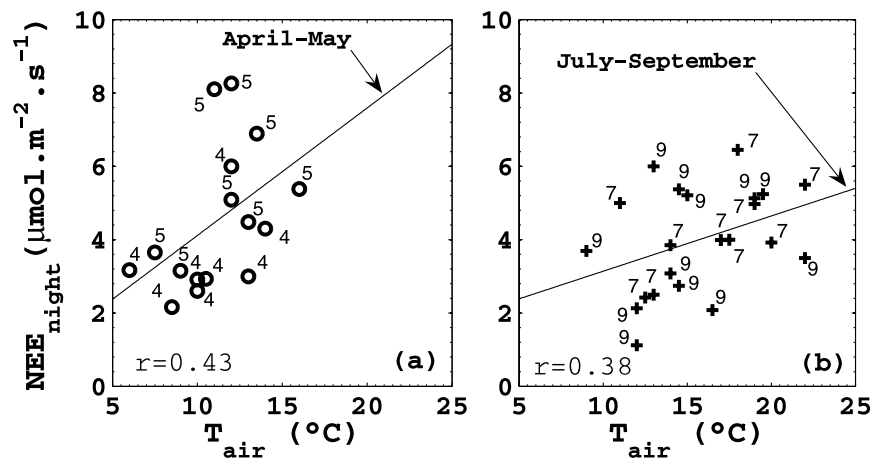


**Figure 12.** Nighttime ecosystem respiration flux retrievals,  $NEE_{night}$ , as a function of the mean air temperature.  $NEE_{night}$  is separated according to the season: April–May corresponds to the spring and the growing season while July–September to the summer.

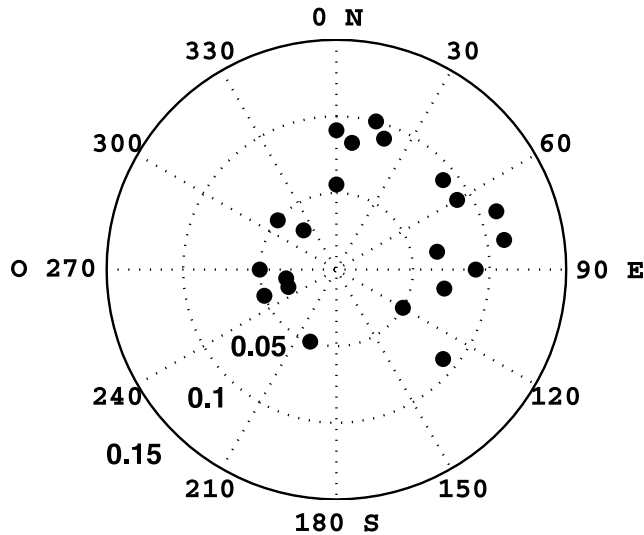


**Figure 13.** Estimates of regional fossil CO<sub>2</sub>/CO emission ratios,  $\eta$  (in parts per million/parts per billion), as a function of the mean ABL wind direction (in degrees).

of wind direction, are displayed in Figure 13. Large values of  $\eta$  close to 0.1 (10 ppb of CO per parts per million of fossil CO<sub>2</sub>) are obtained when the wind blows from the northeast. Under these conditions, the IPSL-LSCE site lies within the Paris pollution plume. A value of 10 ppb ppm<sup>-1</sup> for the CO to fossil CO<sub>2</sub> mixing ratio is close to the one determined for car traffic emissions by *Braud et al.* [2004], which lends support to our ABL method to separate fossil from natural contributions (and fluxes).

## 7. Uncertainty Analysis

### 7.1. Error Analysis on ABL Height Estimation

[40] The accuracy of  $M$  and NEE is linked to the one of ABL height estimates from lidar measurements and radiosoundings [equations (1)-(3), (5)-(6)]. To study the NBL height ( $h_{NBL}$ ) uncertainties, we compared coincident radiosoundings from LMD and Trappes between 18 May and 8 June. The temporal error was estimated by the variance of  $h_{NBL}$  at each site during one night. The spatial error was estimated from the variance of the NBL and ML heights calculated from distant radiosoundings at the same time. Table 2 summarizes the different error sources on the ABL height retrieval. The relative error on  $h_{NBL}$  is larger compared with that on the ML height. In the potential temperature and lidar signals, the limit NBL-RL is usually less marked than the RL-FA interface which is marked by a strong temperature inversion. During the night, the NBL height may vary in thickness by displacing the bottom of the

RL. These variations are linked to horizontal wind speed variations and wave motions [*Stull*, 1988]. A small increase in  $h_{NBL}$  during the night hence explains the large uncertainty ( $\pm 15\%$ ) caused by temporal variability (Table 2).

### 7.2. Error Analysis on $NEE_{night}$ Retrieval

[41] To link the linear increase of nighttime CO<sub>2</sub> mixing ratio and the  $NEE_{night}$ , we need to know the vertical gradient of CO<sub>2</sub> into the NBL. In this study, we make the hypothesis that all NBL scalars (CO<sub>2</sub>, H<sub>2</sub>O...) follow the same gradient than the vertical potential temperature. In order to quantify the possible errors brought by this hypothesis, we chose to compare experimental and modeled [using the potential temperature profile and equation (6)] specific humidity profiles (Figure 14a). The relative error on the mean specific humidity in the NBL is given in Figure 14b. Except for 4 days among the 21 studied, the use of the NBL potential temperature profile to predict the specific humidity one causes an error of less than 10%.

[42] The relative error on  $NEE_{night}$  also depends on  $h_{NBL}$  and  $\alpha$ . To estimate the errors on these parameters, we assumed an exponential decrease of CO<sub>2</sub> with height:

$$C(z, t) = [C(0, t) - C_{RL}] \exp(-z/l) \quad (7)$$

where  $l \approx h_{NBL}/3$  and  $C(0, t)$  is the CO<sub>2</sub> mixing ratio from ground-based in situ measurement.

[43] Using equations (5) and (7), we obtain:

$$NEE_{night} = \rho l \frac{d}{dt} \left[ \int_0^{h_{NBL}} (C(0, t) - C_{RL}) \exp(-z/l) dz \right] \quad (8)$$

Then,

$$NEE_{night} = \rho l \frac{dC(0, t)}{dt} [1 - \exp(-h_{NBL}/l)] \quad (9)$$

The relative error on the respiration flux is:

$$\frac{\sigma(NEE_{night})}{NEE_{night}} = \frac{\sigma(a)}{a} + 3 \frac{\sigma(h_{NBL})}{h_{NBL}} \left[ \frac{e^{-3}}{1 - e^{-3}} \right] \quad (10)$$

where  $a = dC(0, t)/dt$  is the slope calculated during the morning and the evening periods (Figure 3). The error on the slope  $\sigma(a)/a$  is mainly due to anthropogenic emissions during the night. Equation (10) shows that the error on  $h_{NBL}$  has only a marginal influence in the total uncertainty ( $\sim 2\%$  for 10% on  $h_{NBL}$ ). This is due to the vertical attenuation of CO<sub>2</sub> with height. At the NBL-RL interface, the CO<sub>2</sub> mixing

**Table 2.** Relative Error on ABL Height Retrieval<sup>a</sup>

	ML Height		NBL Height		
	Lidar	RS: Spatial Error, LMD-Trappes	RS: Temporal error		RS: Spatial Error, LMD-Trappes
			LMD	Trappes	
$\delta(h)/h$	0.05	0.05	0.17	0.12	0.11

<sup>a</sup>Lidar backscatter signal and radiosoundings at both facilities, LMD and Trappes, were used to estimate the spatial and temporal representativity of the ABL height. LMD and Trappes facilities are separated by 10 km.

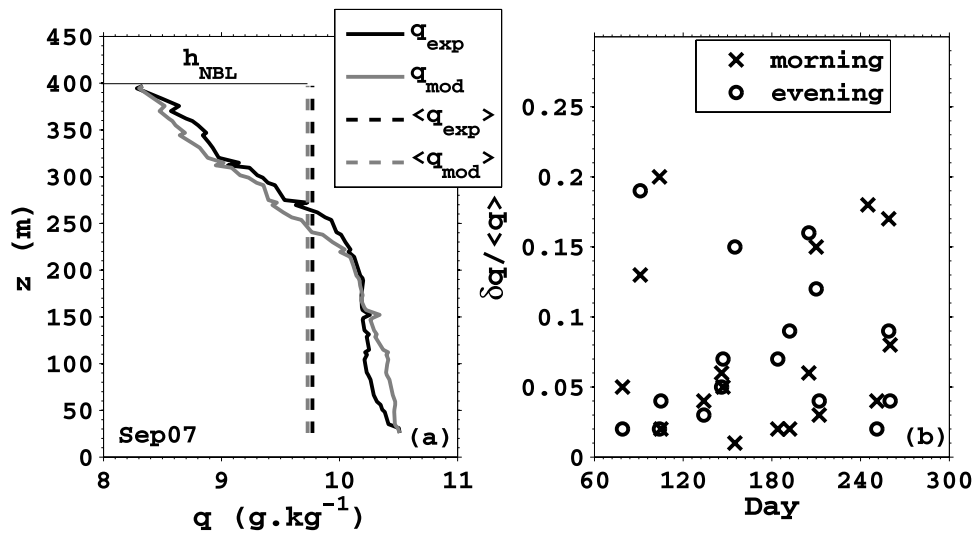


**Figure 14.** (a) Experimental and modeled (from potential temperature profile) vertical specific humidity profiles in the NBL using Trappes 7 September-2300 UT radiosounding. (b) Relative error on the mean NBL specific humidity using potential temperature profile along the year 2004.

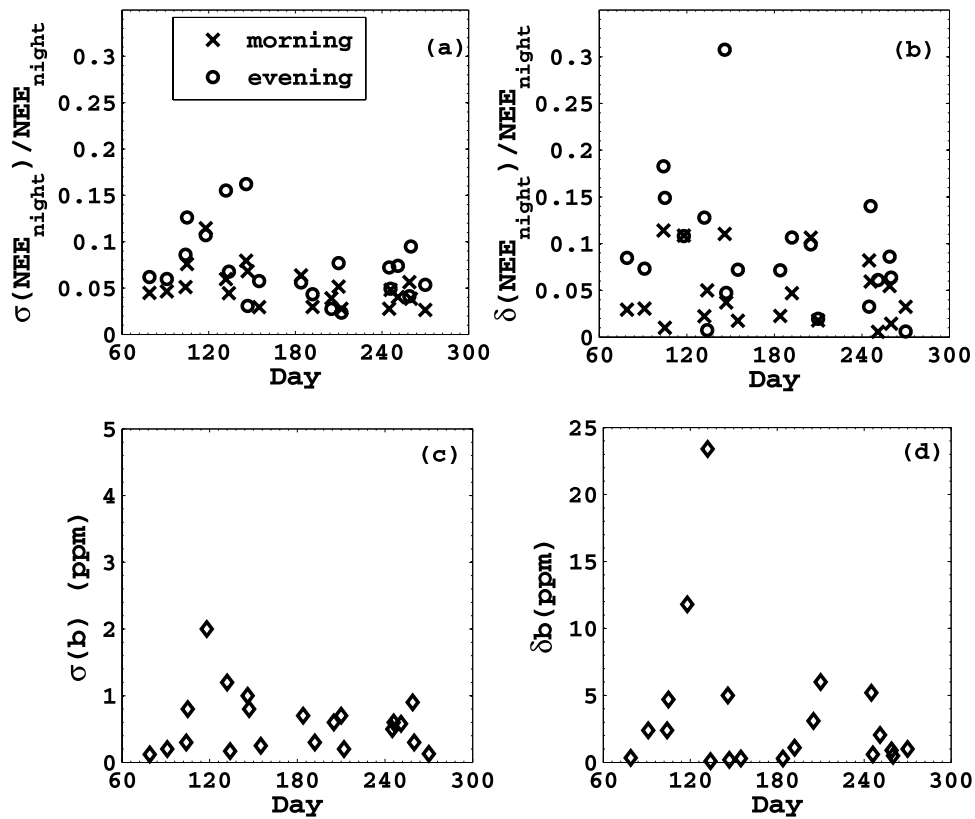


**Figure 15.** (a) Statistical relative error on  $NEE_{night}$  calculations from slope estimates during the morning and the evening. (b) Systematic error on  $NEE_{night}$  due to a correction of CO<sub>2</sub> ground-based in situ measurements from anthropogenic emission, assuming a 1 ppm of anthropogenic CO<sub>2</sub> from 10 ppb of CO. (c) Statistical error on  $b$  calculation from the linear fit taken during the morning period (see also Figure 3). (d) Systematic error on  $b$  due to the trapping of anthropogenic emissions of CO<sub>2</sub> in the NBL during the night and assuming a 1 ppm of CO<sub>2</sub> from 10 ppb of CO.

**Table 3.** Initial and Prescribed Error Values for the Input Parameters  $h$ ,  $R$ ,  $C(0, 0)$ , and  $C_+$  and Result Errors on the Outputs  $C$ ,  $P$ , and  $M$  After Monte-Carlo Simulations

Inputs				Outputs		
$\sigma(h)/h$	$\sigma(\beta)/\beta$	$\sigma(C(0, 0))$ , ppm	$\sigma(C_+)$ , ppm	$\sigma(C)$ , ppm	$\sigma(NEE_{day})/NEE_{day}$	$\sigma(M)/M$
0.05	–	–	–	<0.3	0.02	0.09
–	0.10	–	–	<1	0.15	0.06
–	–	2.0	–	<2	0.06	0.09
–	–	–	0.5	<0.3	0.08	0.07
0.05	0.10	2.0	0.5	<2.5	0.16	0.13

ratios are similar. Therefore  $NEE_{night}$  estimate is only weakly sensitive to variations in  $h_{NBL}$ . Then, we obtain:

$$\frac{\sigma(NEE_{night})}{NEE_{night}} \approx \frac{\sigma(a)}{a} \quad (11)$$

[44] Figure 15a shows the relative error on  $NEE_{night}$  for the morning and the evening periods.

[45] The error on  $NEE_{night}$  is on the order of  $\sim 10\%$ . The evening period is often contaminated by car traffic emissions which add a bias on the slope  $a$  (Figure 15b). However,

this error remains below  $\sim 15\%$ . During the night, the anthropogenic emissions induce an error that is close to the statistical error in the least squares fit. Thus the value of  $a$  proves to be rather insensitive to the anthropogenic emissions (see also Figure 3).

### 7.3. Uncertainty on the First Point: $\delta C(0, 0)$

[46] The first point of modeled CO<sub>2</sub> diurnal cycle  $C(0, 0)$  equals the intercept  $b$  of the linear fit to the CO<sub>2</sub> data displayed (Figure 3). Anthropogenic emissions influence the value of  $b$ . The statistical error on  $b$  is small ( $< 1$  ppm)

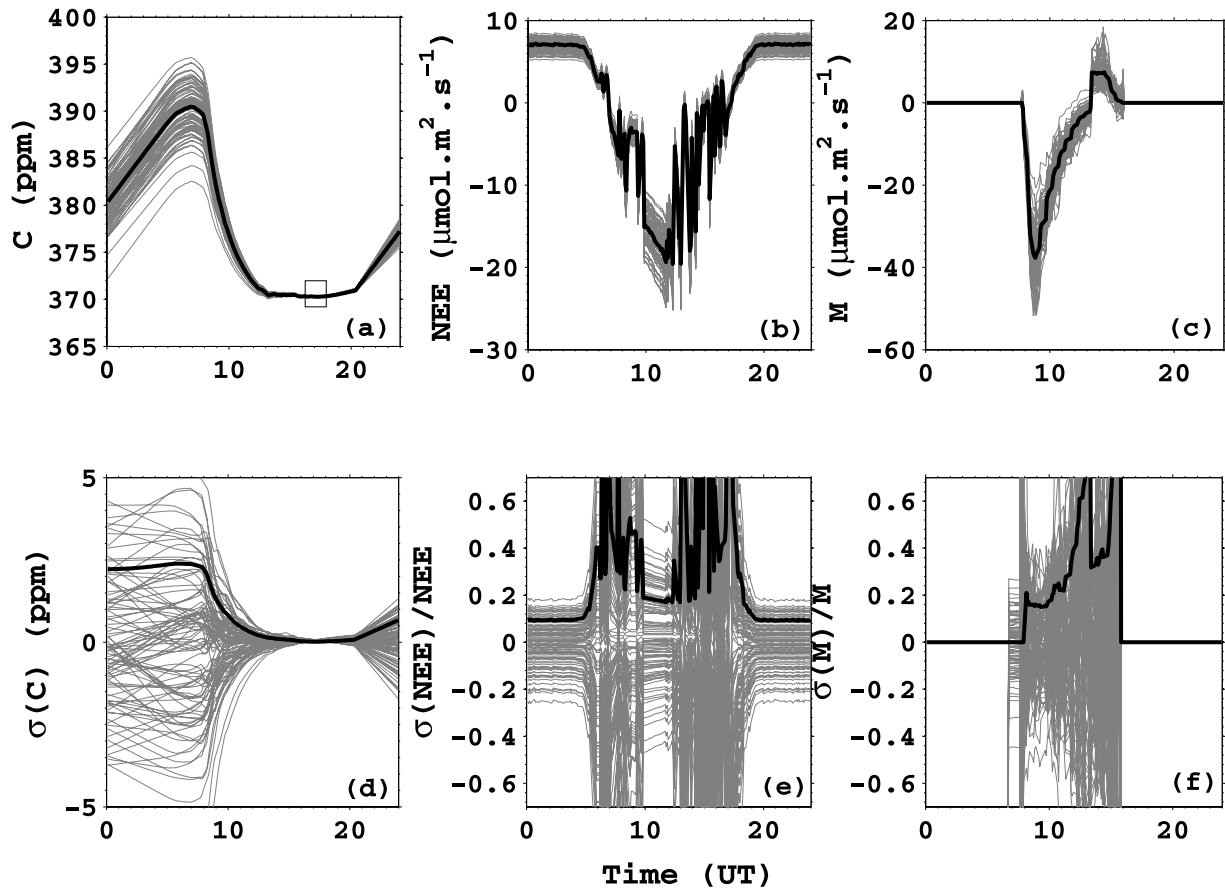


**Figure 16.** Monte-Carlo simulations modeling the 30 July case and assuming that  $\sigma(C(0, 0)) = 2$  ppm,  $\sigma(\beta)/\beta = 0.1$ ,  $\sigma(h)/h = 0.05$ , and  $\sigma(C_+) = 0.5$  ppm. Initial inputs (a–c) and standard deviation (d–f) are indicated in dark and bold solid lines, respectively. (a) Ground-based CO<sub>2</sub> mixing ratio diurnal cycle. (b)  $NEE$ , net ecosystem exchange. (c)  $M$ , vertical mixing flux. (d–f) Errors on  $C$ ,  $NEE_{day}$ , and  $M$  due to Monte-Carlo simulations.

(Figure 15c). However, if the NBL traps anthropogenic emissions of the day before, the value of  $b$  would be higher. Assuming an average ratio  $\eta$  of 0.1, the effect of anthropogenic sources on the value of the intercept (parameter  $\delta b$ ) can be estimated (Figure 15d). The mean value of  $\delta b$  is 3.5 ppm. In total, we estimate the total error on  $C(0, 0)$  to be less than 2 ppm, owing mostly to the systematic error on  $\delta b$  caused by anthropogenic emissions of the day before.

#### 7.4. Monte-Carlo Analysis of Errors on $M$ and $NEE_{day}$ Fluxes

[47] Monte-Carlo simulations were performed to analyze the sensitivity of  $M$  and  $NEE_{day}$  to the model input parameters (Figure 5). The values for  $\beta$ ,  $h$ ,  $C(0, 0)$ , and  $C_+$  are chosen randomly with a Gaussian distribution of half-width equal to each parameter's standard deviation (Table 3). The initial and prescribed CO<sub>2</sub> are those of 30 July (see Figure 16a). The mean value of  $\beta$  is prescribed to  $7 \mu\text{mol m}^{-2} \text{s}^{-1}$  (equaled to the nighttime NEE).

[48] Although the uncertainty on  $C(0, 0)$  appears to be large, it has a small impact on the inference of  $NEE_{day}$  [ $\pm 6\%$  for an error on  $C(0, 0)$  of ppm]. Actually, this offset is usually reduced during the ABL rise in the morning by vertical mixing with air aloft in the RL and FA. Therefore an error on  $C(0, 0)$  entails a significant error on  $M$  [ $\pm 9\%$  for  $\sigma(C(0, 0)) = 2$  ppm]. The retrieval of  $M$  is also sensitive to errors on the CO<sub>2</sub> mixing ratio in the RL and FA. A random error on  $C_+$  estimated to be  $\pm 0.5$  ppm adds an error of 7% to the estimated value of  $M$ . Finally, the values of  $NEE_{day}$  and  $NEE_{night}$ , i.e.,  $\beta$ , are highly correlated. For a 10% relative error on  $R$ , the relative errors on  $NEE_{day}$  and  $M$  are of 15 and 6%, respectively (Table 3).

[49] Assuming  $1 - \sigma$  Gaussian errors for  $\sigma(C(0, 0)) = 2 \pm \sigma(\beta)/\beta = 0.1$ ,  $\sigma(h)/h = 0.05$ , and  $\sigma(C_+) = 0.5$  ppm, we made 100 Monte-Carlo simulations. The results are given in Figure 16 and Table 3. The total error estimate on  $M$  is 13% mainly due to uncertainties in ABL height and in  $\delta C(0, 0)$ . The error on the modeled CO<sub>2</sub> diurnal variation is also due to uncertainties in  $\delta C(0, 0)$ . Finally, the relative errors on  $NEE_{day}$  is found to be on the order of 15%.

## 8. Conclusion

[50] A method based on boundary layer budgeting and observations from various in situ and remote sensing instruments has been developed to infer regional NEE in presence of nearby anthropogenic sources. Measurements of CO<sub>2</sub> within and above the ABL, in conjunction with a precise knowledge of the change in ABL height by lidar, enabled to infer the dependency of NEE on solar radiation. The retrieved seasonal course of NEE follows the course of the growing season, whereas the entrainment flux of CO<sub>2</sub> is rather linked to the heating of the surface. The diurnal flux variations show that the morning decrease of CO<sub>2</sub> mixing ratio is mainly due to a vertical mixing between the NBL and the residual layer first and then with the free troposphere. Sources of  $5 \mu\text{mol m}^{-2} \text{s}^{-1}$  during the night and sinks of  $-20 \mu\text{mol m}^{-2} \text{s}^{-1}$  for NEE in the middle of the day in May are in good agreement with nearby eddy-covariance data. The light conversion factor was found to increase with a larger fraction of diffuse solar radiation.

[51] Lidar backscatter proved to be very user changes in ABL height. One direction for further work is to improve

the capability of the lidar to profile the lower part of the ABL near the surface. This will provide some information about height and gradients in the NBL that could be compared with vertical distribution of various scalars of interest such as potential temperature and specific humidity.

[52] This study also opens the way to direct measurement of CO<sub>2</sub> mesoscale fluxes using a DIAL system. Indeed, DIAL instrument can simultaneously provide mean CO<sub>2</sub> measurements in the ABL, aerosol backscatter signal to retrieve the vertical structure of the ABL and velocity information.

[53] **Acknowledgments.** We thank Pierre Cellier (INRA, Grignon, France) for providing the INRA flux measurements and Jun-Ichi Yano (CNRM, Météo-France, Toulouse, France) and Kenneth J. Davis (The Pennsylvania State University, USA) for critically reading the manuscript.

## References

- Anthoni, P. M., A. Knohl, C. Rebmann, A. Freibauer, M. Mund, W. Ziegler, O. Kolle, and E.-D. Schulze (2004a), Forest and agricultural land-use-dependent CO<sub>2</sub> exchange in Thuringia, Germany, *Glob. Change Biol.*, *10*, 2005–2019.
- Anthoni, P. M., A. Freibauer, O. Kolle, and E.-D. Schulze (2004b), Winter wheat carbon exchange in Thuringia, Germany, *Agric. For. Meteorol.*, *121*(1–2), 55–67.
- Baldocchi, D., R. Valentini, S. Running, W. Oechel, and R. Dahlman (1996), Strategies for measuring and modelling carbon dioxide and water vapour fluxes over terrestrial ecosystems, *Glob. Change Biol.*, *2*, 159–168.
- Bakwin, P. S., P. P. Tans, B. B. Stephens, S. C. Wofsy, C. Gerbig, and A. Grainger (2003), Strategies for measurements of atmospheric column means of carbon dioxide from aircraft using discrete sampling, *J. Geophys. Res.*, *108*(D16), 4514, doi:10.1029/2002JD003306.
- Bakwin, P. S., K. J. Davis, C. Yi, S. C. Wofsy, J. W. Munger, L. Haszpra, and Z. Barcza (2004), Regional carbon dioxide fluxes from mixing ratio data, *Tellus*, *56B*, 301–311.
- Braud, H., P. Bousquet, and M. Ramonet (2004), *CO/CO<sub>2</sub> Ratio in Urban Atmosphere: Example of the Agglomeration of Paris, France*, no. 42, Institut Pierre Simon Laplace (IPSL), Notes des Activités Instrumentales (N.A.I), Paris.
- Crisp, D., et al. (2004), The Orbiting Carbon Observatory (OCO) Mission, *Adv. Space Res.*, *34*, 700–703, Manuscript No. A1.2-0007-02.
- Davis, K. J., P. S. Bakwin, C. Yi, B. W. Berger, C. Zhaos, R. M. Teclaw, and J. G. Isebrands (2003), The annual cycles of CO<sub>2</sub> and H<sub>2</sub>O exchange over a northern mixed forest as observed from a very tall tower, *Glob. Change Biol.*, *9*, 1278–1293.
- de Arellano, J. V.-G., B. Gioli, F. Miglietta, H. J. J. Jonker, H. K. Baltink, R. W. A. Hutjes, and A. A. M. Holtslag (2004), Entrainment process of carbon dioxide in the atmospheric boundary layer, *J. Geophys. Res.*, *109*, D18110, doi:10.1029/2004JD004725.
- Dolman, A. J., R. Ronda, F. Miglietta, and P. Ciais (2005), Regional measurement and modelling of carbon balances, in *The Carbon Balance of Forest Biomes*, edited by H. Griffiths and P. G. Jarvis, Taylor and Francis, Philadelphia, Pa.
- Gerbig, C., J. C. Lin, S. C. Wofsy, B. C. Daube, A. E. Andrews, B. B. Stephens, P. S. Bakwin, and C. A. Grainger (2003), Toward constraining regional-scale fluxes of CO<sub>2</sub> with atmospheric observations over a continent: 2. Analysis of COBRA data using a receptor-oriented framework, *J. Geophys. Res.*, *108*(D24), 4756, doi:10.1029/2002JD003018.
- Gibert, F., P. H. Flamant, D. Bruneau, and C. Loth (2006), Two-micrometer heterodyne differential absorption lidar measurements of the atmospheric CO<sub>2</sub> mixing ratio in the boundary layer, *Appl. Opt.*, *45*, 4448–4458.
- Gloor, M., S.-M. Fans, S. Pacala, J. Sarmiento, and M. Ramonet (1999), A model-based evaluation of inversions of atmospheric transport, using annual mean mixing ratios, as a tool to monitor fluxes of nonreactive trace substances like CO<sub>2</sub> on a continental scale, *J. Geophys. Res.*, *104*(12), 14,245–14,260.
- Granier, A., K. Pilegaard, and N. O. Jensen (2002), Similar net ecosystem exchange of beech stands located in France and Denmark, *Agric. For. Meteorol.*, *114*, 75–82.
- Gu, L., D. Baldocchi, S. B. Verma, T. A. Black, T. Vesala, E. M. Falge, and P. R. Dowty (2002), Advantages of diffuse radiation for terrestrial ecosystem productivity, *J. Geophys. Res.*, *107*(D6), doi:10.1029/2001JD001242.
- Helliker, B. R., J. A. Berry, A. K. Betts, P. S. Bakwin, K. J. Davis, A. S. Denning, J. R. Ehleringer, J. B. Miller, M. P. Butler, and D. M. Ricciuto (2004), Estimates of net CO<sub>2</sub> flux by application of

- equilibrium boundary layer concepts to CO<sub>2</sub> and water vapor measurements from a tall tower, *J. Geophys. Res.*, *109*, D20106, doi:10.1029/2004JD004532.
- Inoue, G. (2005), The greenhouse gases monitoring in-situ and from space (GOSAT), paper presented at 13th Coherent Laser Radar Conference, Kamakura, Japan.
- Kätterer, T., M. Reichstein, O. Andren, and A. Lomander (1998), Temperature dependence of organic matter decomposition: A critical review using literature data analysed with different models, *Biol. Fertil. Soils*, *27*, 258–262.
- Levy, P. E., A. Grelle, A. Lindroth, M. Mölder, P. G. Jarvis, B. Kruijt, and J. B. Moncrieff (1999), Regional scale CO<sub>2</sub> fluxes over central Sweden by a boundary layer budget method, *Agric. For. Meteorol.*, *98-99*, 169–180.
- Lloyd, J., and J. Taylor (1994), On the temperature dependence of soil respiration, *Funct. Ecol.*, *8*, 315–323.
- Lloyd, J., et al. (2001), Vertical profiles, boundary layer budgets, and regional flux estimates for CO<sub>2</sub> and its <sup>13</sup>C/<sup>12</sup>C ratio and for water vapor above a forest/bog mosaic in central Siberia, *Glob. Biogeochem. Cycles*, *15*(2), 267–284.
- Menut, L., C. Flamant, J. Pelon, and P. H. Flamant (1999), Urban boundary layer height determination from lidar measurements over the Paris area, *Appl. Opt.*, *38*, 945–954.
- Miglietta, F., B. Gioli, R. W. A. Hutjes, and M. Reichstein (2006), Net regional ecosystem CO<sub>2</sub> exchange from airborne and ground-based eddy-covariance, land-use maps and weather observations, *Glob. Change Biol.*, doi:10.1111/j.1365-2486.2006.01219.
- Min, Q. (2005), Impact of aerosols and clouds on forest-atmosphere carbon exchange, *J. Geophys. Res.*, *110*, D06203, doi:10.1029/2004JD004858.
- Moureaux, C., A. Debacq, B. Bodson, B. Heinesch, and M. Aubinet (2006), Annual net ecosystem carbon exchange by a sugar beet crop, *Agric. For. Meteorol.*, *139*, 25–39.
- Pépin, L., M. Schmidt, M. Ramonet, D. Worthy, and P. Ciais (2002), *A New Gas Chromatographic Experiment to Analyze Greenhouse Gases in Flask Samples and in Ambient Air in the Region of Saclay*, no. 12, Institut Pierre Simon Laplace (IPSL), Notes des Activités Instrumentales (N.A.I.), Paris.
- Perrin, D., E. Laitat, M. Yernaux, and M. Aubinet (2004), Modelling of the response of forest soil respiration fluxes to the main climatic variables, *Biotechnol. Agron. Soc. Environ.*, *8*, 15–25.
- Reichstein, M., et al. (2003), Modelling temporal and large-scale spatial variability of soil respiration from soil water availability, temperature and vegetation productivity indices, *Glob. Biogeochem. Cycles*, *17*(4), 1104.
- Stull, R. B. (1988), *An Introduction to Boundary Layer Meteorology*, Springer, New York.
- Turner, D. P., S. V. Ollinger, and J. S. Kimball (2004), Integrating remote sensing and ecosystem process models for landscape to regional scale analysis of the carbon cycle, *BioScience*, *54*, 573–584.
- Valentini, R., et al. (2000), Respiration as a main determinant of carbon balance in European forests, *Nature*, *404*, 861–865.
- Wofsy, S. C., M. L. Goulden, J. M. Munger, S. M. Fan, and P. S. Bakwin (1993), Net exchange of CO<sub>2</sub> in a mid-latitude forest, *Science*, *260*, 1314–1317.
- Worthy, D. E. J., I. Levin, N. B. A. Trivett, A. J. Kuhlmann, J. F. Hopper, and M. K. Ernst (1998), Seven years of continuous methane observations at a remote boreal site in Ontario, Canada, *J. Geophys. Res.*, *103*(D13), 15995–16007.
- Yi, C., K. J. Davis, P. S. Bakwin, B. W. Berger, and L. C. Marr (2000), Influence of advection on measurements of the net ecosystem-atmosphere exchange of CO<sub>2</sub> from a very tall tower, *J. Geophys. Res.*, *105*, 9991–9999.
- Yi, C., K. J. Davis, P. S. Bakwin, A. S. Denning, N. Zhang, A. Desai, J. C. Lin, and C. Gerbig (2004), Observed covariance between ecosystem carbon exchange and atmospheric boundary layer dynamics at a site in northern Wisconsin, *J. Geophys. Res.*, *109*, D08302, doi:10.1029/2003JD004164.

---

P. Ciais, M. Ramonet, M. Schmidt, and I. Xueref, Institut Pierre Simon Laplace, Laboratoire des Sciences du Climat et de l'Environnement, UMR CEA/CNRS 1572, C.E. de l'Orme des Merisiers, 91191, Gif-sur-Yvette, Cedex, France.

J. Cuesta, P. H. Flamant, and F. Gibert, Institut Pierre Simon Laplace, Laboratoire de Météorologie Dynamique, Ecole Polytechnique, 91128, Palaiseau, Cedex, France. (fabien.gibert@lmd.polytechnique.fr)

E. Larmanou, INRA Unité Mixte de Recherche INRA/INAPG "Environnement et Grandes Cultures", 78850, Thiverval-Grignon, France.